Scilight

Environmental and Microbial Technology
https://www.sciltp.com/journals/emt

Article

Check for updates

Microenvironmental Engineering of a Solid-State Electrolyte Reactor for Efficient Microbial Electrosynthesis of Acetate from CO_2

Na Chu [1,†], Xiaobing Wu [2,†], Weihong Zheng [2], Yanwei Luo [2], Hang Lin [2], Bingjie Sun [2], Huilin Chen [2], Chenghao Xu [2], Yan Wang [2], Xintong Xu [2], Jiping Tang [2,*], Yaoxing Liu [1] and Yong Jiang [2,*]

[1] Fujian Key Laboratory of Pollution Control and Resource Reuse, College of Environmental and Resource Sciences, Fujian Normal University, Fuzhou 350117, China
[2] Fujian Provincial Key Laboratory of Soil Environmental Health and Regulation, College of Resources and Environment, Fujian Agriculture and Forestry University, Fuzhou 350002, China
* Correspondence: jpt80027@foxmail.com (J.T.); jiangyongchange@163.com or jiangyongchange@fafu.edu.cn (Y.J.)
† These authors contributed equally to this work.

How To Cite: Chu, N.; Wu, X.; Zheng, W.; et al. Microenvironmental Engineering of a Solid-State Electrolyte Reactor for Efficient Microbial Electrosynthesis of Acetate from CO_2. *Environmental and Microbial Technology* **2026**, *1*(1), 11. https://doi.org/10.53941/emt.2026.100011

Received: 17 February 2026
Revised: 27 March 2026
Accepted: 31 March 2026
Published: 13 April 2026

Abstract: Tandem systems coupling electrochemical CO_2 reduction (CO_2RR) with microbial conversion offer a promising strategy to overcome the limitations of conventional microbial electrosynthesis (MES), which typically suffers from low reaction rates due to its reliance on electrode–biofilm architectures. In this study, we develop a solid-state electrolyte (SSE) reactor through microenvironmental engineering, eliminating the need for prefabricated anion exchange membranes (AEMs) and advanced electrocatalysts—both of which have constrained the practical deployment of SSE systems. A potassium-infused, sandwich-structured gas diffusion electrode (GDE) is fabricated via a three-layer, layer-by-layer assembly, an approach shown to be superior to the physical mixing of any two of the constituent layers. Furthermore, a simple filter paper separator is employed in place of pristine or porous AEMs to mitigate hydrogen accumulation and maintain a pH gradient at the GDE–SSE interface. Using commercial bismuth nanoparticles as the electrocatalyst, this configuration enables stable operation for over 130 h, yielding more than 3 litres of pure formic acid solution at concentrations exceeding 0.1 M. For microbial conversion, the integrated system achieves a near-theoretical formate-to-acetate molar ratio of 4.1:1 with a pure acetogenic culture, while a mixed consortium yields a slightly higher ratio of 5.0:1. This work underscores the potential of microenvironmental engineering in advancing cost-effective tandem systems for CO_2 valorization.

Keywords: CO_2 electrolysis; microenvironmental engineering; acetogen; gas diffusion electrode; formic acid

1. Introduction

The escalating challenges of climate change and energy scarcity, driven by the extensive combustion of fossil fuels, have motivated the development of technologies that convert CO_2 into chemical energy using electrical power. Microbial electrosynthesis (MES) is an electro-microbial production platform that employs electrical energy to drive microbial metabolism, enabling the conversion of CO_2 into multicarbon organic compounds [1–3]. Recognized for its mild operational conditions, high selectivity for multi-electron products, tolerance to impurities, and extended operational longevity, MES is considered a promising third-generation green biomanufacturing

technology [4]. The performance of MES hinges on the design of an efficient electrochemical–microbial cascade. Conventional MES systems primarily rely on electrode–biofilm architectures, where electron transfer to microorganisms occurs via direct electron transfer (DET) or hydrogen-mediated indirect electron transfer. However, DET is constrained by the limited number of cathodic electrotrophs, biofilm thickness, and cellular electron consumption rates, typically resulting in current densities below 1 mA cm^{-2} [5,6]. Consequently, substantial research efforts in MES have focused on developing cathode materials to enhance conductivity and biocompatibility [7]. Hydrogen-mediated electron transfer, which couples electrochemical hydrogen evolution with microbial H_2 assimilation, faces challenges such as low gas–liquid mass transfer efficiency and safety concerns. To address these, reactor designs incorporating extended flow paths have been explored to increase hydrogen residence time and improve product formation [8].

In recent years, electrochemical CO_2 reduction (CO_2RR) has garnered significant attention as a viable route for chemical synthesis under mild conditions [9–11]. For two-electron products such as formate, CO_2RR can achieve current densities one to three orders of magnitude higher than those in conventional MES, primarily due to the use of gas diffusion electrodes (GDEs) that overcome mass transport limitations [6]. Nevertheless, its selectivity for multi-electron products like acetate and methane remains limited, often necessitating sophisticated electrocatalyst fabrication processes that are challenging to scale [12].

Efforts to integrate CO_2RR electrocatalysts into MES date back to 2012 [13]. Notably, formate serves as a soluble electron mediator that circumvents the gas–liquid mass transfer and safety issues associated with H_2 or CO, while also acting as a favourable carbon source for microbial catalysts such as acetogens. However, the shared catholyte in such configurations imposes a key limitation, complicating the simultaneous optimization of electrochemical activity and microbial biocompatibility and preventing substantial increases in current density [6]. CO_2RR typically employs concentrated electrolytes such as $KHCO_3$ or KOH (≥1 M) to suppress the hydrogen evolution reaction (HER), but these conditions can cause microbial cell lysis [14]. Moreover, the harsh electrochemical environment, including electric field gradients and the generation of reactive species, can induce microbial apoptosis. Additionally, electrolyte composition critically influences CO_2RR performance, and impurities present in microbial culture media (e.g., Fe and Mn) may poison electrocatalysts [15].

A tandem reactor strategy, involving sequential catalytic steps, can effectively decouple electrocatalytic formate production from microbial formate utilization. This approach theoretically enables independent optimization of the two processes, thereby enhancing overall MES performance [16,17]. However, when conventional CO_2RR reactors are employed in such tandem systems, the liquid products (i.e., formate) are typically mixed with high-concentration catholytes [18], inhibiting downstream microbial conversion and failing to resolve biocompatibility issues.

Solid-state electrolyte (SSE) reactors offer a transformative approach to CO_2RR [19–21], enabling the direct generation of high-purity formic acid as a bioavailable feedstock without contamination by high-concentration electrolytes [20,22,23]. The core operation of a conventional SSE reactor involves four key processes: (i) ion-exchange membranes separate the anode and cathode, with an SSE layer containing ion-exchange resin positioned between them; (ii) formate generated at the cathode migrates through an anion exchange membrane (AEM); (iii) protons released at the anode transport through a cation exchange membrane (CEM); and (iv) neutralization occurs within the SSE layer, where deionized water facilitates the extraction of high-purity formic acid.

Despite these advantages, the practical deployment of SSE reactors has been hindered by their reliance on prefabricated AEMs and advanced electrocatalysts. Most SSE studies utilize expensive AEMs such as Sustainion X37-50 (Dioxide Materials, Boca Raton, FL, USA) to facilitate anion transport [20]. Additionally, considerable effort has been devoted to developing high-performance electrocatalysts for SSE systems, including Bi-based metal–organic frameworks [24], Cu–Bi nanorod array catalyst [20], and active sites modified with anionic groups [23]. Thus, the dependence on prefabricated AEMs and advanced electrocatalysts has constrained the development of a mature tandem reactor strategy for electro-microbial production. Recent progress in microenvironmental engineering, which involves tailoring local reaction conditions rather than relying solely on high-cost components or advanced electrocatalysts, offers an alternative pathway to improve electrochemical performance through enhanced substrate accessibility, stabilization of key intermediates, and modulation of local reaction environments [25–27]. These insights provide a foundation for designing next-generation SSE reactors with standardized operation and reduced overall costs.

In this study, we employ microenvironmental engineering to eliminate the need for both prefabricated AEMs and advanced electrocatalysts, thereby reducing the capital cost of SSE reactors. We demonstrate the necessity of a sandwich electrode architecture and elucidate the role of the separator material in preventing the formation of insulating hydrogen gas layers and maintaining a pH gradient. The system utilizes pure formic acid as an intermediary to bridge the electrochemical and microbial stages, resolving biocompatibility issues while

leveraging the high reaction rate of CO_2RR and the high selectivity of microbial catalysts. This work provides a viable pathway towards cost-effective and scalable SSE reactors, advancing CO_2 valorization through electro-microbial processes.

2. Materials and Methods

2.1. Layer-by-Layer Construction of GDEs

Three distinct layer-by-layer fabrication methods were employed to prepare the GDEs (Figure 1a), with abbreviations and full descriptions provided in Table S1:

- Method 1: Incorporation of Potassium into the Catalytic Layer Followed by Polymer Deposition

Commercial bismuth nanoparticles (WOWMATERIALS, Changzhou, China) and carbon black (optimized mass ratio of 3.5) were dispersed in isopropanol, Sustainion polymer solution, and varying volumes (133, 200, 400, 600, or 800 µL) of 0.15 M KOH solution to prepare the conductive ink. The ink was uniformly sprayed onto a gas diffusion layer (GDL, 4 cm^2, sigracet 39 BB, SGL Carbon, Wiesbaden, Germany) to form a Bi/C GDE with a catalyst loading of approximately 3.0 mg cm^{-2}. Subsequently, a polymer coating was applied by spraying 1200 µL of a polymer solution (200 µL of 5% Sustainion or Nafion mixed with 1000 µL of ethanol) onto the GDE.

- Method 2: Sequential Deposition of the Catalytic Layer and Potassium-Doped Polymer Solution

The Bi/C GDE was fabricated as in Method 1, but using an ink without KOH solution for the coating. A polymer solution containing 1200 µL of Sustainion (200 µL of 5% Sustainion + 1000 µL ethanol) and varying volumes (133, 200, 400, 600, or 800 µL) of 0.15 M KOH was then sprayed onto the Bi/C GDE.

- Method 3: Cation-Infused Sandwich Structure

This method involved the sequential deposition of three distinct layers: a catalytic layer, a potassium layer, and a polymer layer. First, the Bi/C GDE was prepared as in Method 2. Varying volumes (133, 200, 400, 600, or 800 µL) of 0.15 M KOH were then sprayed to form the potassium layer, followed by the deposition of 1200 µL of Sustainion (200 µL of 5% Sustainion + 1000 µL ethanol) to form the polymer layer.

The fabricated GDEs were evaluated in an SSE reactor for pure formic acid production from CO_2RR (Figure S1). The anode consisted of platinum-coated titanium felt [28], and the SSE layer was composed of a strong cation-exchange resin (Amberlite® IRC120, Sigma-Aldrich, St. Louis, MO, USA). The anode solution comprised 100 mL of 0.5 M H_2SO_4, and the SSE layer was supplied with deionized water in single-pass mode for formic acid extraction. The gas chamber was continuously fed with 50 sccm of dry CO_2. The anode solution flow rate was 2 mL min^{-1}, while the deionized water flow rate was maintained at 0.26 mL min^{-1}. The SSE reactor was operated at a fixed cell voltage of 4.0 V. Notably, no separator was placed between the GDE and the SSE layer in the initial setup.

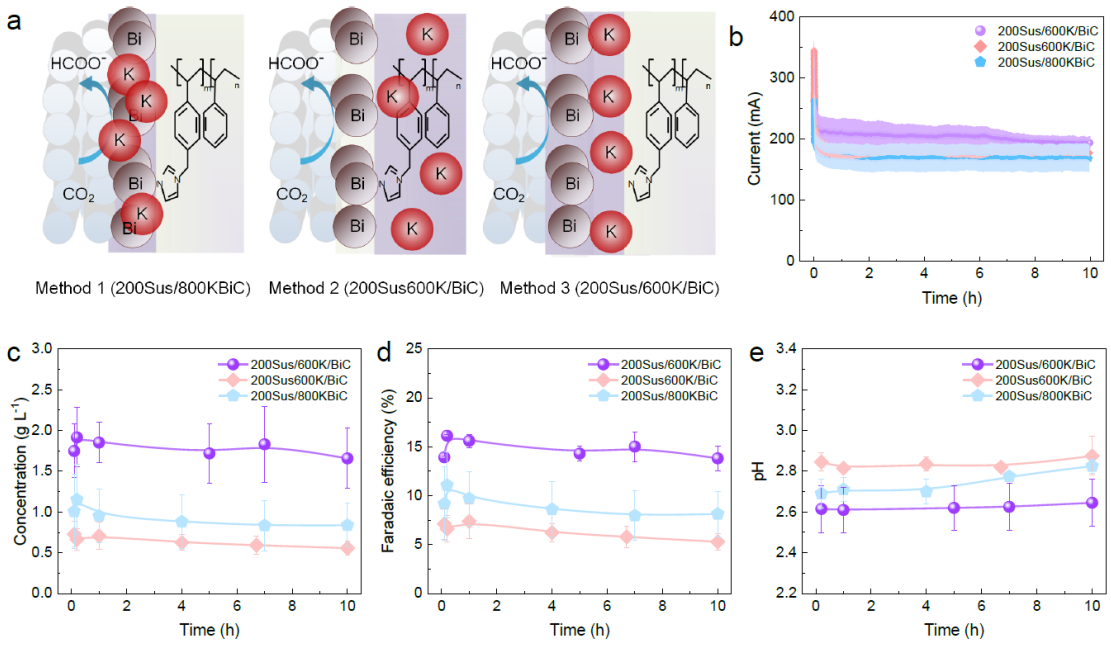

Figure 1. Comparison of the three GDE preparation methods: (**a**) schematic diagram of preparation methods and electrodes prepared under optimal conditions; (**b**) Current density; (**c**) Formic acid concentration; (**d**) FE; and (**e**) pH of the extracted solution.

2.2. Construction of the SSE Reactor Using Pristine or Porous AEMs

The cation-infused sandwich-structured GDE was utilized in the SSE reactor, operated under the same conditions described in Section 2.1. The only modification was the insertion of either a pristine or porous AEM (FAA-3-PK-130, Fumasep, Sinero Technology Co., Suzhou, China) between the GDE and the SSE layer. To create a porous AEM, a needle roller (Micro Skin Beauty System 540-0.3, Biotulin, MyVitalSkin GmbH & Co. KG, Aachen, Germany) was employed, offering a relatively simple and effective alternative to conventional techniques such as phase inversion or electrospinning [29].

2.3. Construction of the SSE Reactor Without Prefabricated AEMs

The cation-infused sandwich-structured GDE was utilized in the SSE reactor, operated under the same conditions described in Section 2.1. The only modification was the insertion of a piece of filter paper (Whatman Grade 1, Cytiva, Marlborough, MA, USA) as the separator instead of a prefabricated AEM. The reactor was operated at a fixed current density of 60 mA cm^{-2}.

2.4. Integrated System Coupling CO_2RR with Subsequent Microbial Conversion

The culture medium for *Acetobacterium woodie* contained the following components: 1.00 g NH_4Cl, 0.33 g KH_2PO_4, 0.45 g K_2HPO_4, 0.10 g $MgSO_4 \cdot 7H_2O$, 20.00 mL modified Wolin's mineral solution, 2.00 g yeast extract, 0.50 mL sodium resazurin (0.1% *w*/*v*), 10.00 g $NaHCO_3$, 1.00 mL Wolin's vitamin solution (10×), 0.50 g L-cysteine $HCl \cdot H_2O$, 0.50 g $Na_2S \cdot 9H_2O$, and 1000 mL distilled water. Formate solutions with concentration gradients, prepared either from chemical reagents or collected directly from SSE reactors, were supplemented into the culture medium. Mixed acetogenic cultures, enriched over an 85-day adaptation period following anaerobic sludge inoculation, were also evaluated [30]. Serum vials were incubated at 30 °C with agitation at 120 rpm.

2.5. Analyses and Calculations

Formic acid concentrations were quantified using high-performance liquid chromatography (HPLC, LC-2030, Shimadzu Scientific Instruments Inc., Kyoto, Japan) [31]. Acetate and other potential carboxylates and alcohols were detected by gas chromatography (Nexis GC-2030, Shimadzu Scientific Instruments Inc., Kyoto, Japan) equipped with a flame ionization detector. Dissolved metal concentrations in the collected formic acid solution were determined via inductively coupled plasma optical emission spectrometry (ICP-OES, Avio 200, PerkinElmer Inc., Waltham, MA, USA). A battery testing system (CT-4008, Neware Technology Co., Ltd., Shenzhen, China) was used to power the electrochemical reactors.

Surface morphology was analyzed using scanning electron microscopy (SEM, ZEISS Sigma 300, ZEISS Group, Oberkochen, Germany), and elemental composition was assessed via energy-dispersive X-ray spectroscopy (EDS, Oxford Xplore 50, Oxford Instruments, Abingdon, UK). Crystal structure was examined using X-ray diffraction (XRD, Rigaku SmartLab SE, Rigaku Corporation, Tokyo, Japan), while hydrophobicity was assessed using a contact angle measurement instrument (SDC 350KS, Kuunshan Sindin Industrial Smart Technology Co., Ltd., Kunshan, China). Cyclic voltammetry (CV) was performed using an electrochemical workstation (CHI 660E, Chenhua Instrument Co., Shanghai, China). The Faradaic efficiency (FE) of the CO_2 electrolysis process was calculated based on a molar conversion factor of 2. Full-cell energy efficiency was used in this study for the assessment of CO_2 electrolyzers. The overall energy efficiency of the integrated system was derived based on the standard heat of combustion of formate (254 kJ mol^{-1}) and acetate (874 kJ mol^{-1}) [31].

3. Results and Discussion

3.1. Performance Evaluation of Layer-by-Layer Constructed GDE Cathodes

For GDEs fabricated using Method 1, where K^+ was introduced into the catalyst layer prior to spraying the Sustainion polymer solution (Figure S2), a decrease in pH following single-pass flow of deionized water through the SSE layer confirmed formic acid formation [32]. However, when the Sustainion polymer layer was replaced with Nafion (200Naf/133KBiC), both formic acid concentration and FE were substantially lower. Moreover, in the absence of a polymer layer, GDE performance deteriorated within the first two hours of operation, indicating the critical role of the polymer layer in enhancing CO_2RR activity.

Differences in molecular structure influence the performance of Nafion and Sustainion ionomers [33]. Nafion is a hydrophobic ionomer due to its fluorinated backbone, whereas Sustainion is more hydrophilic owing to the presence of strong polar groups. Consequently, Sustainion primarily enhances CO_2 concentration at the catalyst

interface, while Nafion membranes mainly increase local pH [34]. Previous studies have demonstrated that coating copper electrodes with Sustainion ionomers enhances C_2H_4 production [35]. Additionally, Sustainion has been shown to inhibit K^+ migration, thereby enhancing ethanol production [36].

GDEs with increasing KOH amounts were tested (Figure S3). The 200Sus/800KBiC configuration exhibited the highest initial formic acid concentration (1.6 g L^{-1}) and FE (14%) at 0.2 h; however, these values gradually stabilized after 10 h of operation. The conductivity of the extracted formic acid solution closely matched that of a standard high-purity formic acid solution, confirming negligible potassium ion release within the tested KOH concentration range [31].

For GDEs fabricated using Method 2, where the catalytic layer was deposited first followed by a potassium-incorporated polymer layer, optimal performance was achieved with the 200Sus600K/BiC configuration (Figure S4). However, the overall FE for formic acid production remained below 10%.

For GDEs fabricated using the cation-infused sandwich structure (Method 3), the 200Sus/600K/BiC configuration yielded the highest formic acid concentration (2.3 g L^{-1}) and Faradaic efficiency (17%) (Figure S5). Gas chromatography analysis revealed H_2 as the sole by-product during CO_2 reduction to formate, with an FE reaching 80%. This selectivity is consistent with the known performance of Bi-based electrocatalysts, which exhibit excellent selectivity for formate production due to their optimal binding affinity for the *OCHO intermediate [37].

For a clearer comparison, GDEs prepared under optimal conditions—200Sus/800KBiC (Method 1), 200Sus600K/BiC (Method 2), and 200Sus/600K/BiC (Method 3)—were tested at a cell voltage of 4 V (Figure 1). Notably, the cation-infused sandwich-structure GDE (Method 3) exhibited superior performance, including higher current density, formic acid concentration, and FE, as well as a significantly lower pH in the collected extraction solution, compared to the other two methods.

Metal content in the extracted formic acid solution was analyzed (Table S2). For GDEs fabricated using Methods 1 and 3, concentrations of Cu, Fe, Na, Bi, and Ag were all below 0.05 mg L^{-1}. In contrast, the GDE prepared using Method 2 exhibited slightly elevated Na and Bi concentrations, although other metals remained below 0.2 mg L^{-1}. Notably, the potassium concentration in the extracted solution was significantly higher for GDEs prepared via Method 2, indicating lower stability and K^+ leaching from the outermost potassium-incorporated polymer layer. Interestingly, for the underperforming GDE prepared using Method 1, the extracted solution contained the lowest metal ion concentrations, highlighting that metrics such as metal leaching do not singularly determine CO_2RR performance [20,23]. CV scans indicated that the superior performance of the cation-infused sandwich-structure GDE was not attributable to an increased electrochemical surface area, as the highest double-layer capacitance (C_{dl}) was obtained for the GDE fabricated using Method 2 (Figure S6).

3.2. Performance of the SSE Reactor with Pristine or Porous AEM Coverage

The performance of the SSE reactor was evaluated by covering the cation-infused sandwich-structured GDE with either a pristine or porous AEM and operating the system at a constant voltage of 4 V. When the pristine AEM was applied directly to the GDE, the current rapidly dropped to 88 mA within the first 5 min of operation (Figure 2a). Applying a single pass of the needle roller to the Fumasep membrane (porous-once) (Figure S7) resulted in higher FE for formic acid (Figure 2b) and a higher formic acid concentration (Figure 2c) compared to applying two passes (porous-twice). However, the current density for the porous-once configuration was lower than that of the porous-twice configuration.

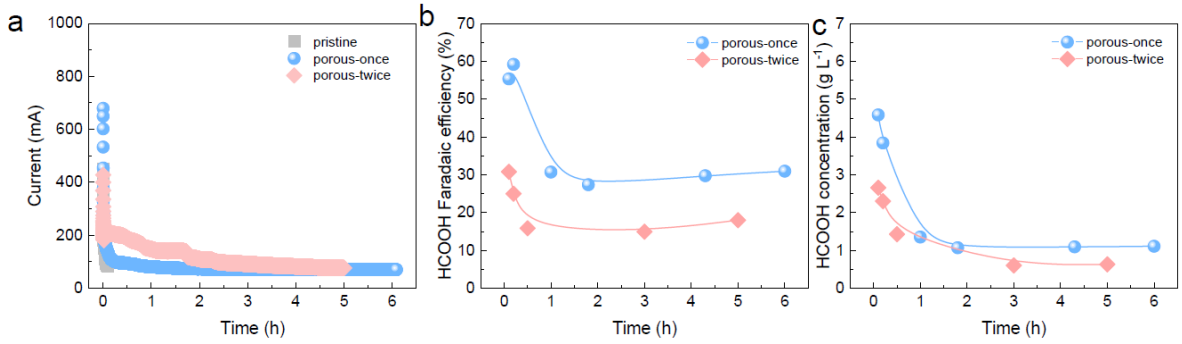

Figure 2. Performance of SSE reactors with GDE covered by pristine or porous AEM: (**a**) Current (**b**) FE and (**c**) concentration.

In SSE reactors, Sustainion membranes are most widely used [23,38] to facilitate formate migration [20] and enhance CO_2RR performance [32,39]. The Fumasep FAA-3-PK-130 membrane is widely employed in flow cells or membrane electrode assemblies (MEAs) due to its greater rigidity and significantly lower cost compared to Sustainion membranes. Despite sporadic reports of Fumasep AEMs in SSE systems [40], our results demonstrate that even with an optimized cation-infused sandwich GDE, covering it with either a pristine or porous Fumasep AEM fails to achieve high CO_2RR performance.

3.3. Performance of the SSE Reactor Free of Prefabricated AEM

We developed the SSE reactor featuring a cation-infused sandwich-structured GDE, with a filter paper layer positioned between the GDE and the SSE layer. The system was operated at a fixed current density of 60 mA cm^{-2} and maintained stable performance for 130 h (Figure 3a). During this period, the FE remained above 40% (Figure 3b), and the pH remained near 2, indicating effective formic acid production (Figure S8). After continuous operation, over 3 L of pure formic acid solution was collected from the SSE reactor (Figure 3c), with a final concentration exceeding 0.1 M (5.12 g L^{-1}). Analysis of the metal content in the collected formic acid solution showed that concentrations of Cu, Fe, K, Na, Bi, and Ag were all below 0.1 mg L^{-1} (Table S3).

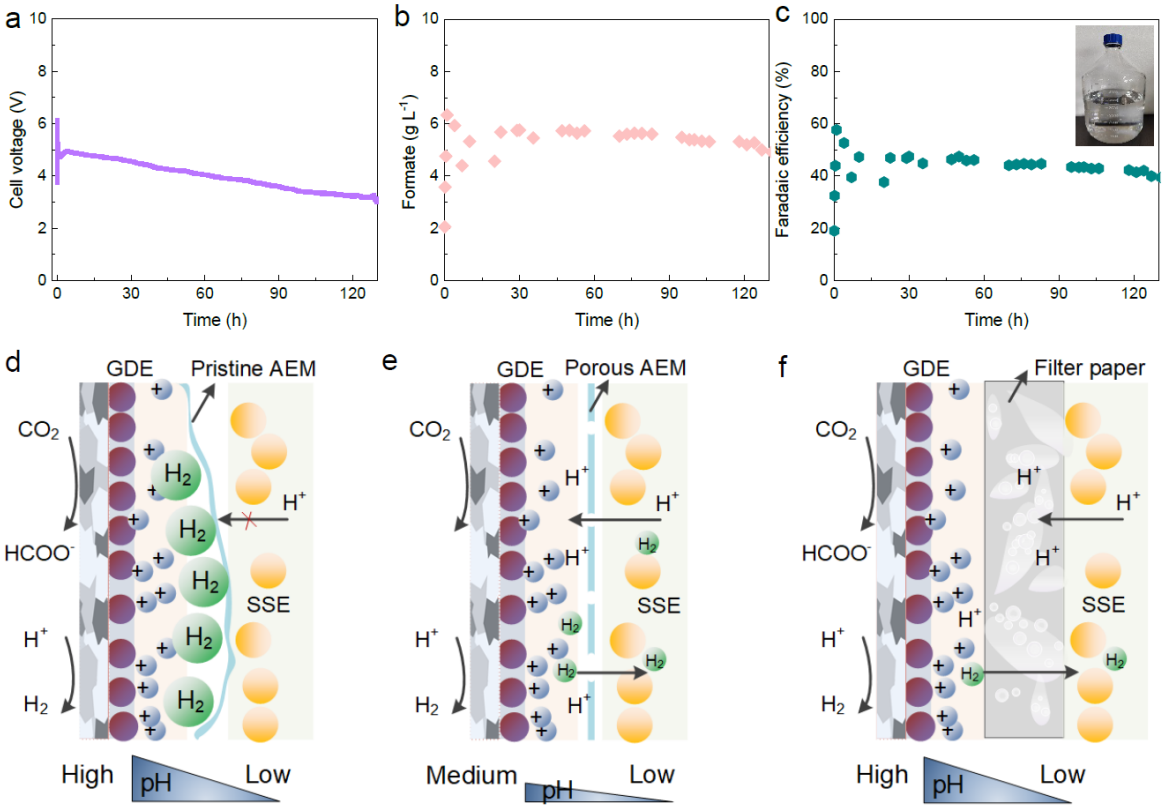

Figure 3. Long-term operation of the SSE reactor free of prefabricated AEM: (**a**) cell voltage; (**b**) Formate concentration; (**c**) FE, and interfacial characteristics between the GDE and SSE when assembled with (**d**) pristine AEM; (**e**) porous AEM; and (**f**) filter paper as separators. The inset shows photographs of over 3 L of pure formic acid solution collected after continuous operation.

The role of different separator materials can be rationalized by considering their interfacial properties. When the pristine AEM was applied directly to the GDE, the rapid current drop was likely due to hydrogen accumulation at the AEM-catalyst interface, increasing internal resistance as this gaseous insulating layer also deformed the AEM (Figure 3d), particularly when suboptimal electrocatalysts were used [30,31]. Recent studies have shown that under HER conditions, hydrogen bubbles can almost entirely cover the GDE surface, and they are larger and detach more slowly than the CO bubbles generated from CO_2RR [41]. When using a porous AEM, while gas removal from the interface can reduce internal resistance, it may also increase proton flux to the catalyst surface, thereby suppressing CO_2RR activity under acidic conditions [26]. In this study, the Fumasep FAA-3-PK-130 membrane, a polyetheretherketone-fabric-reinforced AEM, is 50 μm thinner than Whatman Grade 1 filter paper (180 μm). More importantly, the fibrous cellulose structure of Whatman filter paper and its appropriate pore size

are likely responsible for establishing a significant pH gradient between the GDE surface (where alkaline conditions favour CO_2RR) and the SSE surface (where the bulk solution pH is typically near 2 due to proton transport from the anode through the CEM). Previous modelling and experimental studies have demonstrated that for the direct electrochemical conversion of carbonate to multicarbon products, filter paper thicknesses that are either too thin or too thick are suboptimal for suppressing HER [42].

Degradation of SSE reactor performance was systematically assessed by examining the pristine sandwich-structured GDE after long-term continuous operation. Photographs comparing the pristine and used GDE revealed notable morphological differences (Figure S9). Cross-sectional EDS elemental mapping revealed that the atomic percentage of potassium decreased from 0.25% in the pristine GDE to 0.01% in the used GDE (Figures 4a,b and S10, Table S4). Interestingly, the contact angle increased from 69.79° in the pristine GDE to 104.18° in the used GDE (Figure 4c), suggesting a shift towards higher surface hydrophobicity. A more hydrophobic surface is known to suppress HER, favouring CO_2-to-formate conversion via the hydride-mediated pathway [20,43].

XRD analysis confirmed that the characteristic peak at approximately 27.6° (Figure 4d), corresponding to metallic Bi(012), remained unchanged in both pristine and used GDEs [31,44]. However, the intensities of the Bi(021) and Bi(024) peaks decreased in the used GDE, while new peaks corresponding to Bi(003), Bi(006), and Bi(107) emerged, indicating subtle alterations in the crystal structure after operation. SEM images of the used GDE showed partial detachment of the coating, increased surface cracking, and the formation of larger particle agglomerates (Figures 4e,f and S11).

In conclusion, long-term operation led to significant physical changes in the GDE, including reduced potassium content and slight modifications in the crystal structure. Despite the increased surface hydrophobicity—which typically benefits stability—these changes collectively contributed to the observed performance degradation.

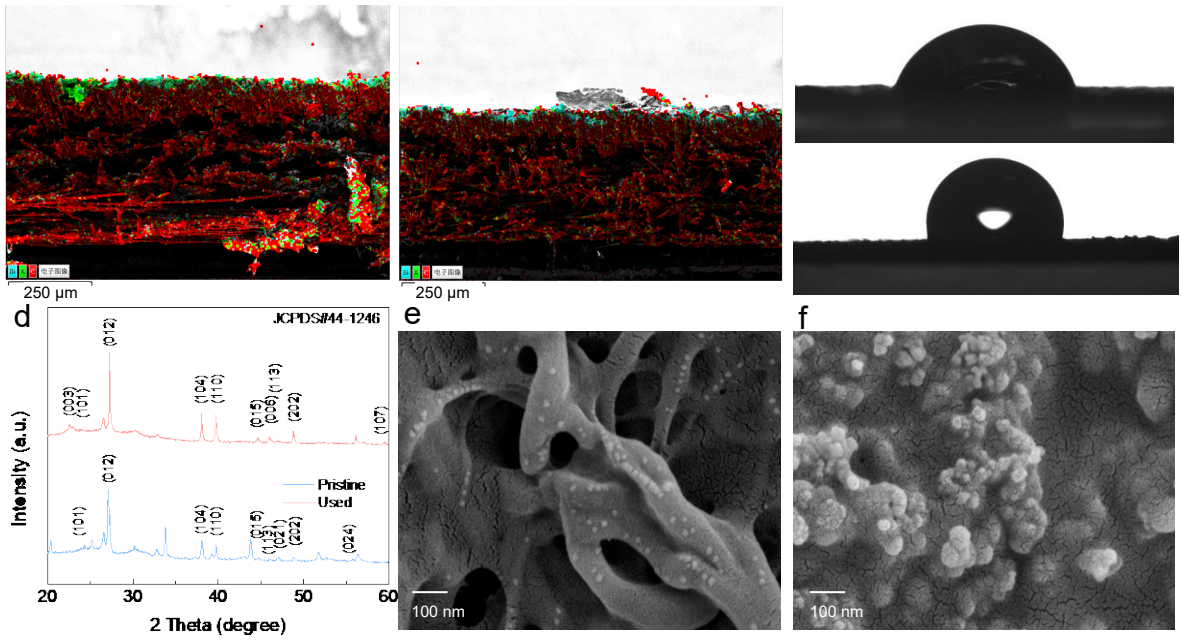

Figure 4. Characterization of the Pristine and Used Sandwich-Structured GDE. Cross-sectional SEM-EDS elemental mapping of (**a**) pristine and (**b**) used GDE. Blue represents Bi, green represents K, and red represents C. (**c**) Contact angle analysis and (**d**) XRD patterns. SEM of (**e**) pristine and (**f**) used GDE.

A performance comparison of pure formic acid production from SSE reactors was conducted (Table S5). While conventional SSE reactors have been reported to operate at current densities as high as 100 mA cm^{-2} [20,45], only a few studies have demonstrated operational stability beyond 100 h [20,46]. For example, while certain electrocatalysts can sustain short-term operation at 100 mA cm^{-2}, long-term stability often requires reducing the current density to 30 mA cm^{-2} for sustained operation [32,39]. Even with advanced electrocatalysts such as carbon-confined indium oxides, reported current densities have been limited to 30 mA cm^{-2}, with stability lasting only 3 h [47]. Similarly, metal(II)-sulfate site electrocatalysts have exhibited current densities below 20 mA cm^{-2} in SSE reactors [23]. Recently, stretched InO_5S electrocatalysts have been developed, achieving CO_2RR in SSE reactors at 20 mA cm^{-2} for 10 h [22]. A recent study also reported a decline in SSE ion exchange capacity over

time, showing that replacing the SSE twice within 7.5 h increased the formic acid concentration in the effluent from 0.2 M to 0.6 M [48].

3.4. Tandem Reactor-Based Microbial Electrosynthesis

Conventional MES systems, whether relying on DET from electrodes to microorganisms, hydrogen-mediated indirect electron transfer, or—as seen in some studies after 2012—the integration of electrocatalysts to reduce CO_2 to formate followed by microbial conversion to acetate in the same catholyte, generally suffer from low current densities (Figure 5a). To address this limitation, we propose a novel system based on an SSE reactor that eliminates the need for both expensive prefabricated AEMs and high-performance advanced electrocatalysts. It utilizes extracted, highly biocompatible pure formic acid as the substrate for cultivating acetogens, thereby establishing a tandem reactor-based electro-microbial production (Figure 5b). Accordingly, the subsequent phase of this work focuses on the efficient microbial upgrading of formic acid to the C_2 product, acetate.

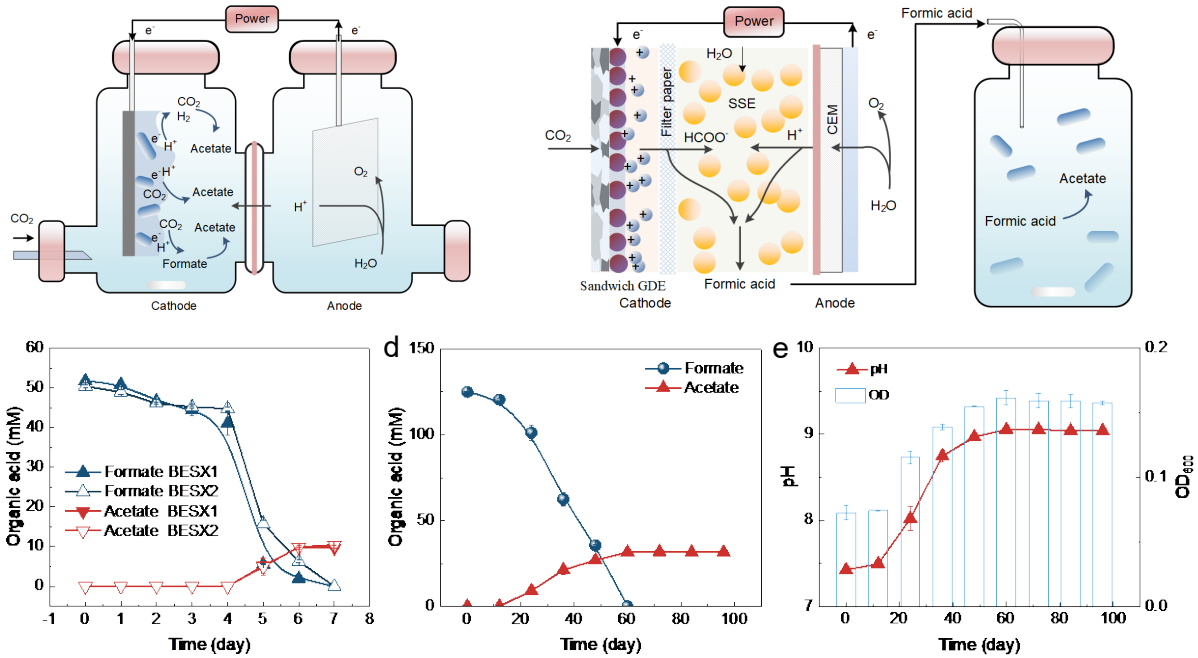

Figure 5. (**a**) Schematic of conventional MES systems. (**b**) Proposed tandem MES process using an SSE reactor for generating biocompatible formate. (**c**) Formate consumption and acetate production using enriched mixed culture supplemented with 1× (2-BES X1) or 2× (2-BES X2) concentration of 2-bromoethanesulfonate. (**d**) Formate consumption and acetate production profiles using *A. woodii* in the tandem system. (**e**) Corresponding pH variation and OD measurements.

First, acetate production by *A. woodie* was evaluated using different initial formate concentrations prepared from chemical reagents. Results showed that across a broad concentration range (50–300 mM), *A. woodie* completely consumed formate within three days, converting it to acetate with high selectivity at a consistent formate-to-acetate molar ratio of 4.1 ± 0.2 (Figure S12). This finding aligns with a previous report indicating a ratio of 4.4:1 when *A. woodii* was grown on 205.5 mM formate [49]. Additionally, it was observed that the initial slightly alkaline medium pH increased to values between 8 and 9 by the end of cultivation, accompanied by an increase in optical density (OD_{600}). This alkalinization during formate consumption by acetogens has been documented elsewhere; for example, the pH reportedly increased from 7.4 to 9.3 during the conversion of 205.5 mM formate [49].

It has been suggested that microbial formate consumption generates OH^-, necessitating acid addition (e.g., HCl) to maintain pH balance [50]. Therefore, the effect of active pH control via HCl addition to maintain the pH below 8 was investigated. However, this pH-regulation strategy did not enhance biomass growth or formate consumption; instead, it slightly delayed acetate production (Figure S13). A possible explanation is that *A. woodii* may be relatively tolerant to pH increases, and the addition of HCl could disturb the microbial microenvironment—for instance, by potentially introducing trace oxygen.

Subsequently, the performance of an enriched mixed culture in converting formate to acetate was examined. Compared with the pure culture, the mixed culture showed a higher formate-to-acetate molar ratio of 5.0 ± 0.3,

despite effective methanogenesis inhibition (Figures 5c and S14). Chromatographic analysis indicated that no volatile fatty acids or alcohols other than formate and acetate were produced during microbial conversion. Therefore, the increased formate-to-acetate molar ratio is more likely attributable to non-acetogenic members of the mixed community consuming part of the formate. Indeed, several natural microbial hosts—including acetogens, methanogens, and *Methylobacterium*—are known to utilize formate [51].

This study further evaluated the performance of *A. woodii* using pure formic acid solution collected from the SSE reactor after continuous operation. The results demonstrated that acetate production did not differ significantly from that achieved using chemical-grade formate (Figure 5d), while the trends in pH variation and OD values remained consistent (Figure 5e).

Using formate/formic acid as the intermediate in tandem reactor-based electro-microbial production offers distinct advantages. First, a flux balance analysis using a core metabolic model indicated that CO_2 fixation pathways initiating with reduction to formate are potentially more ATP-efficient and support higher biomass yields than pathways relying solely on carboxylation [52]. Consistently, the energetic efficiency of acetogenic growth on formate is reportedly higher than on the more conventional substrate, H_2 [50]. Second, CO_2 that is not electrochemically reduced or is re-released by microbial processes may positively influence the microbial conversion process. For example, carbonate/bicarbonate has been shown to enhance acetate production and reduce H_2 release in *A. woodii* during formate conversion [49].

Based on the 130 h of stable operation, the energy efficiency of the SSE reactor, calculated from the input electrical energy and the chemical energy of the produced formate, was determined to be 14.0%. The energy losses are primarily attributable to the high internal resistance. Compared to zero-gap configurations, the ion-exchange resin layer, while facilitating ion transport, contributes significantly to the overall internal resistance. Additionally, the filter paper, which is essential for maintaining the pH gradient, also contributes to the internal resistance. Energy efficiencies ranging from 7% to 48% have been reported for conventional SSE cells, albeit under varying operating conditions, SSE dimensions, packing densities, and current densities [53–56]. It is important to note that energy efficiencies reported in the literature based on theoretical cell voltage or half-cell (cathode) potentials are generally higher than those based on combustion heat. Notably, this study avoids the use of expensive prefabricated AEMs and utilizes commercially available, scalable electrocatalysts. Furthermore, the produced formic acid is not mixed with cations, reducing downstream product separation costs, which partially offsets the energy conversion losses. The overall energy efficiency of the coupled electrochemical–microbial system (chemical energy of acetate product/input electrical energy) was calculated to be 11.7% for the pure culture and 9.6% for the mixed culture. The SSE reactor in this study was not specifically optimized for CO_2 conversion efficiency. However, the bulk acidic conditions within the SSE layer can improve carbon utilization efficiency in CO_2RR through the neutralization of HCO_3^-/CO_3^{2-} by H^+ and subsequent regeneration of CO_2, thus potentially achieving higher CO_2 utilization than under alkaline or neutral conditions. In practice, the carbon conversion efficiency of all CO_2RR reactors is strongly dependent on the CO_2 flow rate [28], necessitating a trade-off with Faradaic efficiency, particularly in the absence of GDEs designed for selective adsorption of low-concentration CO_2. In conventional SSE systems, CO_2 released from carbonate after passing through the AEM cannot be re-electro-reduced. Our system resembles an acidic CO_2RR configuration without soluble alkali metal cations, utilizing an SSE layer. Assuming a carbon utilization rate of at least 40% without significant compromise in formic acid Faradaic efficiency—while the highest reported value in the literature can reach 75% [53]—the overall carbon utilization of the coupled system (carbon in acetate product/input CO_2) was estimated to be approximately 20% for the pure culture and 16% for the mixed culture.

A quantitative techno-economic analysis for HCOOH production in SSE reactors has recently been conducted, demonstrating a 14.4% lower cost compared to acidic CO_2RR, primarily due to the absence of product separation expenses, indicating that SSE reactors represent the most promising electrolyzer configuration [53,57]. The electro-microbial coupling system proposed in this study offers several advantages over existing CO_2 conversion technologies. The electrochemical stage operates under mild ambient conditions, can be directly powered by sustainable energy sources, and does not require expensive AEMs or non-scalable high-performance electrocatalysts. The electron carrier generated electrochemically is not mixed with high concentrations of cations, allowing its direct use as a microbial substrate without inhibiting microbial activity. The spatial separation of the electrochemical and microbial stages prevents mutual inhibition, and the biological stage utilizes inexpensive, renewable microbial catalysts. However, given that carbon capture credits do not currently have a strong economic impact and considering the energy costs for synthesizing the energy carrier, as well as other capital and operating costs, products from electro-microbial production must be sold for at least approximately \$2 kg^{-1} of product. However, most major commodities such as staple crops (e.g., wheat, rice, maize), feed, fuels, and bulk chemicals are currently at or below the approximately \$1 kg^{-1} producer or wholesale price [3]. Therefore, from an economic

perspective, integrating new functionalities and expanding applications is crucial. The pure formic acid generated by the novel SSE reactor in this study, besides serving as a substrate for microbial production of organic acids, could also be used in other applications, such as a carbon source for denitrification in wastewater treatment. The oxygen generated at the anode could be utilized for pure oxygen aeration in wastewater treatment [58], although this typically relies on scarce noble metals. Our results indicate an urgent need to improve the energy efficiency of the system. Therefore, the oxygen evolution reaction could be replaced with organic oxidation processes, such as the valorization of biomass-derived substrates or the oxidation of plastic hydrolysates, to recover valuable products and reduce energy consumption [59]. Future work could also focus on developing high-performance synthetic microbial chassis via synthetic biology to enable efficient CO_2 conversion into value-added products.

4. Conclusions

In this study, a novel SSE reactor was developed that eliminates the need for prefabricated AEMs and advanced electrocatalysts through the application of microenvironmental engineering techniques. Among the GDEs evaluated, the cation-infused sandwich-structured design exhibited superior performance. Further investigation revealed that covering the GDE with either pristine or porous Fumasep AEMs did not yield high CO_2RR performance in the SSE reactor. However, integrating a filter paper separator between the GDE and the SSE layer resulted in stable operation for over 130 h by relieving interfacial hydrogen accumulation and maintaining a pH gradient. Long-term operation led to significant changes in surface topography, a reduction in potassium content, and slight modifications in the crystal structure, which outweighed the benefits of increased surface hydrophobicity. Although the electro-microbial coupling system achieved a near-theoretical formate-to-acetate molar ratio of 4.1:1 with a pure acetogen, the use of a mixed consortium resulted in a slightly increased ratio of 5.0. Future research should focus on further exploring the scalability of the reactor, expanding its environmental applications, or designing engineered microbial strains to achieve higher-value products.

Supplementary Materials

The additional data and information can be downloaded at: https://media.sciltp.com/articles/others/260410 0950284594/EMT-26020100-SM.pdf. Figure S1: Three-chamber solid electrolyte reactor. (a) Photograph and (b) GDE and (c) middle chamber. Figure S2: The performance of GDE prepared using method 1. (a) Current; (b) formate concentration; (c) Faradic efficiency and (d) pH. Figure S3: Potassium concentration of GDE prepared using method 1 was optimized. (a) Current; (b) formate concentration; (c) Faradic efficiency and (d) conductivity. Figure S4: The performance of GDE prepared using method 2. (a) current; (b) formate concentration; (c) Faradic efficiency and (d) conductivity. Figure S5: The performance of GDE prepared using method 3. (a) current; (b) formate concentration; (c) Faradic efficiency and (d) conductivity. Figure S6: CV of GDE prepared with: (a) Method 1; (b) Method 2; (c) Method 3 and (d) Calculation of double-layer capacitance (C_{dl}) from CV curves. Figure S7: Photographs of the porous AEM, prepared by applying (a) a single pass (porous-once) or (b) two passes (porous-twice) of the needle roller on the Fumasep membrane. Figure S8: The pH of pure formic acid solution collected from the solid electrolyte reactor free of prefabricated AEM during continuous operation. Figure S9: Photographs of the cation-infused sandwich-structured GDE: (a) pristine and (b) after long-term continuous operation with some filter paper fragments adhering to the surface. Figure S10: Cross-sectional EDS elemental mapping of (a–c) pristine and (d–f) after long-term continuous operation. Figure S11: SEM of the cation-infused sandwich-structured GDE: (a) pristine and (b) after long-term continuous operation. Figure S12: The effect of initial formate concentration on the acetogenesis performance of *A. woodii*. Key performance indicators monitored include: (a) formate consumption; (b) acetate production; (c) medium pH; and (d) bacterial growth (OD600). Figure S13: During formate conversion using *A. woodii*, the pH was maintained below 8 by the addition of HCl. The key performance indicators monitored were: (a) formate consumption; (b) acetate production; (c) medium pH, and (d) bacterial growth (OD600). Figure S14: The enriched mixed culture for formate conversion was supplemented with 1× (2-BES X1) or 2× (2-BES X2) concentration of 2-bromoethanesulfonate: (a) Gas proportion in the 2-BES X1 group and (b) Gas proportion in the 2-BES X2 group. Table S1: Abbreviations and full names of GDE corresponding to preparation methods. Table S2: Metal content of the collected formic acid solution at 0.5, 4.5 and 9.5 h during operation using GDE papered with different methods (Method 1, Method 2, and Method 3). Table S3: Metal content in formic acid solution after over 130 h of continuous operation with 200Sus/600K/BiC at 240 mA. Table S4: Cross-sectional EDS mapping analysis of different GDE samples. Table S5: Performance comparation of pure formic acid production from SSE reactors. References [60–69] are cited in supplementary materials.

Author Contributions

N.C. and X.W.: Writing—original draft preparation, investigation; W.Z.: Investigation; Y.L. (Yanwei Luo), H.L., B.S., H.C., C.X., Y.W. and X.X.: Formal analysist; J.T.: Investigation, conceptualization; Y.L. (Yaoxing Liu): Formal analysist; Y.Y.: Writing—original draft, investigation, funding acquisition, formal analysis. All authors have read and agreed to the published version of the manuscript.

Funding

This work was supported by the National Natural Science Foundation of China (52500026, 52370033), Natural Science Foundation of Fujian Province (2025J08145, 2024J010021).

Institutional Review Board Statement

Not applicable.

Informed Consent Statement

Not applicable.

Data Availability Statement

Data will be made available on request.

Conflicts of Interest

The authors declare no conflict of interest.

Use of AI and AI-Assisted Technologies

During the preparation of this work, the authors used Deepseek and ChatGPT to proofread for grammatical errors. After using this tool/service, the authors reviewed and edited the content as needed and take full responsibility for the content of the published article.

References

1. Kuang, M.; Li, B.; Zhou, L.; et al. Carbon Dioxide Upgrading to Biodegradable Plastics through Photo/Electro-Synthetic Biohybrid Systems. *Angew. Chem. Int. Ed.* **2025**, *64*, e202422357.
2. Ying, Z.; Qiu, Q.; Ye, J.; et al. Mechanism, Performance Enhancement, and Economic Feasibility of CO_2 Microbial Electrosynthesis Systems: A Data-Driven Analysis of Research Topics and Trends. *Renew. Sust. Energy Rev.* **2024**, *202*, 114704.
3. Lovat, S.J.; Ben-Nissan, R.; Milshtein, E.; et al. Electro-Microbial Production Techno-Economic Viability and Environmental Implications. *Nat. Biotechnol.* **2025**, *43*, 848–853.
4. Liu, Z.; Wang, K.; Chen, Y.; et al. Third-Generation Biorefineries as the Means to Produce Fuels and Chemicals from CO_2. *Nat. Catal.* **2020**, *3*, 274–288.
5. Jourdin, L.; Grieger, T.; Monetti, J.; et al. High Acetic Acid Production Rate Obtained by Microbial Electrosynthesis from Carbon Dioxide. *Environ. Sci. Technol.* **2015**, *49*, 13566–13574.
6. Chu, N.; Jiang, Y.; Liang, Q.; et al. Electricity-Driven Microbial Metabolism of Carbon and Nitrogen: A Waste-to-Resource Solution. *Environ. Sci. Technol.* **2023**, *57*, 4379–4395.
7. Shakeel, S.; Khan, M.Z.; Shakeel, M. Microbial Electrosynthesis of Acetic Acid from Carbon Dioxide Using a Bimetallic-Granular Activated Carbon Cathode. *Bioelectrochemistry* **2026**, *168*, 109158.
8. Bian, B.; Ma, X.; Li, S.; et al. Microbial Electrosynthesis of Methane in an Up-Scaled Zero-Gap Cell. *Water Res.* **2026**, *297*, 125723.
9. Li, L.; Ye, W.; Liu, Q.; et al. Operando Raman Characterization of Unique Electroinduced Molecular Tautomerization in Zero-Gap Electrolyzers Promotes CO_2 Reduction. *Proc. Natl. Acad. Sci. USA* **2025**, *122*, e2418144122.
10. Pham, T.H.; Lai, H.D.T.; Dang, N.K.; et al. Ambipolar Ion Transport Membranes Enable Stable Noble-Metal-Free CO_2 Electrolysis in Neutral Media. *Adv. Energy Mater.* **2025**, *15*, e04286.
11. Wang, Z.; Wang, W.; Yang, Q.; et al. Highly Selective Acidic CO_2 Electroreduction with Large Current on Polypyrrole-Modified Ag Catalyst by Local Microenvironment Modulation. *Adv. Energy Mater.* **2025**, *15*, 2405419.
12. Lv, Z.; Wang, C.; Liu, W.; et al. Enhanced CO_2 Adsorption and Conversion in Diethanolamine-Cu Interfaces Achieving Stable Neutral Ethylene Electrosynthesis. *Adv. Energy Mater.* **2024**, *14*, 2402551.

13. Li, H.; Opgenorth, P.H.; Wernick, D.G.; et al. Integrated Electromicrobial Conversion of CO_2 to Higher Alcohols. *Science* **2012**, *335*, 1596.
14. Hann, E.C.; Overa, S.; Harland-Dunaway, M.; et al. A Hybrid Inorganic–Biological Artificial Photosynthesis System for Energy-Efficient Food Production. *Nat. Food* **2022**, *3*, 461–471.
15. Staerz, A.F.; van Leeuwen, M.; Priamushko, T.; et al. Effects of Iron Species on Low Temperature CO_2 Electrolyzers. *Angew. Chem. Int. Ed.* **2024**, *63*, e202306503.
16. Cui, H.; Liu, W.; Ma, C.; et al. Converting CO_2 to Single-Cell Protein via an Integrated Electrocatalytic-Biosynthetic System. *Appl. Catal. B Environ. Energy* **2024**, *350*, 123946.
17. Lee, G.; Jo, H.J.; Choi, J.; et al. CO_2 Upgrading into Bioproducts Using a Two-Step Abiotic-Biotic System. *Proc. Natl. Acad. Sci. USA* **2025**, *122*, e2512565122.
18. Jiang, Y.; Wu, G.; Pu, Y.; et al. Flow-Electrode Capacitive Separation of Organic Acid Products and Recovery of Alkali Cations after Acidic CO_2 Electrolysis. *Proc. Natl. Acad. Sci. USA* **2024**, *121*, e2408205121.
19. Zhu, P.; Wu, Z.Y.; Elgazzar, A.; et al. Continuous Carbon Capture in an Electrochemical Solid-Electrolyte Reactor. *Nature* **2023**, *618*, 959–966.
20. Zhang, G.; Tan, B.; Mok, D.H.; et al. Electrifying HCOOH Synthesis from CO_2 Building Blocks over Cu-Bi Nanorod Arrays. *Proc. Natl. Acad. Sci. USA* **2024**, *121*, e2400898121.
21. Chu, N.; Jiang, Y.; Zeng, R.J.; et al. Solid Electrolytes for Low-Temperature Carbon Dioxide Valorization: A Review. *Environ. Sci. Technol.* **2024**, *58*, 10881–10896.
22. Sun, Y.; Dai, L.; Sui, N.L.D.; et al. Direct Parallel Electrosynthesis of High-Value Chemicals from Atmospheric Components on Symmetry-Breaking Indium Sites. *Proc. Natl. Acad. Sci. USA* **2024**, *121*, e2409620121.
23. Yuan, C.Y.; Feng, L.; Qin, X.; et al. Constructing Metal(II)-Sulfate Site Catalysts toward Low Overpotential Carbon Dioxide Electroreduction to Fuel Chemicals. *Angew. Chem. Int. Ed.* **2024**, *63*, e202405255.
24. Zhao, Z.H.; Huang, J.R.; Huang, D.S.; et al. Efficient Capture and Electroreduction of Dilute CO_2 into Highly Pure and Concentrated Formic Acid Aqueous Solution. *J. Am. Chem. Soc.* **2024**, *146*, 14349–14356.
25. Ma, M.; Seger, B. Rational Design of Local Reaction Environment for Electrocatalytic Conversion of CO_2 into Multicarbon Products. *Angew. Chem. Int. Ed.* **2024**, *63*, e202401185.
26. Zeng, M.; Fang, W.; Cen, Y.; et al. Reaction Environment Regulation for Electrocatalytic CO_2 Reduction in Acids. *Angew. Chem. Int. Ed.* **2024**, *63*, e202404574.
27. Liu, J.; Xie, S.; Li, D.; et al. Microenvironmental Hydrophobicity-Regulated Evolution of Reaction Sites for Boosting Electrochemical CO_2 Reduction. *Appl. Catal. B Environ. Energy* **2025**, *379*, 125700.
28. Pu, Y.; Wang, Y.; Wu, G.; et al. Tandem Acidic CO_2 Electrolysis Coupled with Syngas Fermentation: A Two-Stage Process for Producing Medium-Chain Fatty Acids. *Environ. Sci. Technol.* **2024**, *58*, 7445–7456.
29. Disch, J.; Ingenhoven, S.; Vierrath, S. Bipolar Membrane with Porous Anion Exchange Layer for Efficient and Long-Term Stable Electrochemical Reduction of CO_2 to CO. *Adv. Energy Mater.* **2023**, *13*, 2301614.
30. Chu, N.; Wu, X.; Zhao, Z.; et al. Biohybrid CO_2 Electrolysis under External Mode: Using Pure Formic Acid Extracted from CO_2 Electroreduction for Diverse Microbial Conversion. *Fundam. Res.* **2025**, *5*, 2597–2606.
31. Chu, N.; Jiang, Y.; Wang, D.; et al. Super-Fast Charging Biohybrid Batteries through a Power-to-Formate-to-Bioelectricity Process by Combining Microbial Electrochemistry and CO_2 Electrolysis. *Angew. Chem. Int. Ed.* **2023**, *62*, e202312147.
32. Xia, C.; Zhu, P.; Jiang, Q.; et al. Continuous Production of Pure Liquid Fuel Solutions via Electrocatalytic CO_2 Reduction Using Solid-Electrolyte Devices. *Nat. Energy* **2019**, *4*, 776–785.
33. Rashid, M.; Nabil, S.K.; Adnan, M.A.; et al. Cation-Infused Bilayer Ionomer Coating Enables High Partial Current Density toward Multi Carbon Products in CO_2 Electrolysis. *Adv. Energy Mater.* **2024**, *14*, 2400570.
34. Kim, C.; Bui, J.C.; Luo, X.; et al. Tailored Catalyst Microenvironments for CO_2 Electroreduction to Multicarbon Products on Copper Using Bilayer Ionomer Coatings. *Nat. Energy* **2021**, *6*, 1026–1034.
35. Li, W.; Yin, Z.; Gao, Z.; et al. Bifunctional Ionomers for Efficient Co-Electrolysis of CO_2 and Pure Water towards Ethylene Production at Industrial-Scale Current Densities. *Nat. Energy* **2022**, *7*, 835–843.
36. Liu, J.; Zhang, B.; Chen, D.; et al. Steering the Selectivity of CORR from Acetate to Ethanol via Tailoring the Thermodynamic Activity of Water. *Angew. Chem. Int. Ed.* **2024**, *63*, e202412266.
37. Zhang, M.; Zhu, W.; Liu, Z.; et al. Selective Sieving Effect of Multi-Atomic Bismuth Interfaces for Efficient Formate Electrosynthesis and Evolution at Industrial Current Density. *Angew. Chem. Int. Ed.* **2025**, *64*, e202510206.
38. Zhu, J.; Li, J.; Lu, R.; et al. Surface Passivation for Highly Active, Selective, Stable, and Scalable CO_2 Electroreduction. *Nat. Commun.* **2023**, *14*, 4670.
39. Fan, L.; Xia, C.; Zhu, P.; et al. Electrochemical CO_2 Reduction to High-Concentration Pure Formic Acid Solutions in an All-Solid-State Reactor. *Nat. Commun.* **2020**, *11*, 3633.
40. Kang, Y.; Kim, Y.; Doh, Y.; et al. Boosting Current Density of Electrocatalytic CO_2 Reduction Using Metal–Enzyme Hybrid Cathodes. *Angew. Chem. Int. Ed.* **2025**, *64*, e202504380.

41. Zhang, Y.; Pan, B.; Li, Y.; et al. Electrochemical pH-Swing CO_2 Capture Facilitated by Suppressed Bubble Accumulation at Electrode/Electrolyte Interfaces. *Angew. Chem. Int. Ed.* **2026**, *65*, e13456.
42. Lee, G.; Rasouli, A.S.; Lee, B.-H.; et al. CO_2 Electroreduction to Multicarbon Products from Carbonate Capture Liquid. *Joule* **2023**, *7*, 1277–1288.
43. Yang, Y.; Zhang, J.; Tan, Z.; et al. Highly Selective Production of C_2^+ Oxygenates from CO_2 in Strongly Acidic Condition by Rough Ag-Cu Electrocatalyst. *Angew. Chem. Int. Ed.* **2024**, *63*, e202408873.
44. Liu, H.; Bai, Y.; Wu, M.; et al. A Regenerable Bi-Based Catalyst for Efficient and Stable Electrochemical CO_2 Reduction to Formate at Industrial Current Densities. *Angew. Chem. Int. Ed.* **2024**, *63*, e202411575.
45. Zheng, T.; Liu, C.; Guo, C.; et al. Copper-Catalysed Exclusive CO_2 to Pure Formic Acid Conversion via Single-Atom Alloying. *Nat. Nanotechnol.* **2021**, *16*, 1386–1393.
46. Zhang, X.; Fang, Z.; Zhu, P.; et al. Electrochemical Regeneration of High-Purity CO_2 from (Bi)carbonates in a Porous Solid Electrolyte Reactor for Efficient Carbon Capture. *Nat. Energy* **2024**, *10*, 55–65.
47. Wang, Z.; Zhou, Y.; Liu, D.; et al. Carbon-Confined Indium Oxides for Efficient Carbon Dioxide Reduction in a Solid-State Electrolyte Flow Cell. *Angew. Chem. Int. Ed.* **2022**, *61*, e202200552.
48. Wang, X.; Zhou, M.; Wang, M.; et al. Copper-Bridge-Enhanced p-Band Center Modulation of Carbon-Bismuth Heterojunction for CO_2 Electroreduction. *Nano Lett.* **2023**, *23*, 10946–10954.
49. Moon, J.; Donig, J.; Kramer, S.; et al. Formate Metabolism in the Acetogenic Bacterium *Acetobacterium woodii*. *Environ. Microbiol.* **2021**, *23*, 4214–4227.
50. Claassens, N.J.; Cotton, C.A.R.; Kopljar, D.; et al. Making Quantitative Sense of Electromicrobial Production. *Nat. Catal.* **2019**, *2*, 437–447.
51. Valentini, F.; Kozell, V.; Petrucci, C.; et al. Formic Acid, a Biomass-Derived Source of Energy and Hydrogen for Biomass Upgrading. *Energy Environ. Sci.* **2019**, *12*, 2646–2664.
52. Cotton, C.A.; Edlich-Muth, C.; Bar-Even, A. Reinforcing Carbon Fixation: CO_2 Reduction Replacing and Supporting Carboxylation. *Curr. Opin. Biotechnol.* **2018**, *49*, 49–56.
53. Hua, Y.; Kang, D.; Huang, J.; et al. Electrified CO_2-to-HCOOH Valorization: A Comparative Technical Analysis on Acidic Flow Cell and Solid-State Electrolyte Cell Reactors. *ACS Energy Lett.* **2026**, *11*, 1880–1888.
54. Xue, J.; Ji, B.; Zhong, K.; et al. Promoted CO_2 Electrolysis to Formic Acid Using Single Atom Cobalt Alloyed Tin. *Adv. Mater.* **2026**, *38*, e72719.
55. Chen, X.; Lu, R.; Li, C.; et al. Activating Inert Non-Defect Sites in Bi Catalysts Using Tensile Strain Engineering for Highly Active CO_2 Electroreduction. *Nat. Commun.* **2025**, *16*, 1927.
56. Adaryan, S.; Wi, T.-U.; Santos, K.; et al. Free-Standing Porous Composite Polyelectrolyte for Efficient CO_2 Electrolysis. *Environ. Sci. Technol.* **2025**, *59*, 26819–26829.
57. Xu, Y.; Zhao, K.; Chang, X.; et al. Emerging Roles of Cations in Electrocatalytic Reduction of CO_2 and CO. *Nat. Energy* **2026**, *11*, 387–399.
58. Liu, Q.; Flores-Alsina, X.; Ramin, E.; et al. Making Waves: Power-to-X for the Water Resource Recovery Facilities of the Future. *Water Res.* **2024**, *257*, 121691.
59. Kormányos, A.; Szirmai, A.; Endrődi, B.; et al. Pairing Electrochemical CO_2 Reduction with Glycerol Oxidation: Bottlenecks Today, Opportunities Tomorrow. *Joule* **2025**, *9*, 102096.
60. Zhang, Y.; Zhang, R.; Chen, F.; et al. Mass-Transfer-Enhanced Hydrophobic Bi Microsheets for Highly Efficient Electroreduction of CO_2 to Pure Formate in a Wide Potential Window. *Appl. Catal. B Environ.* **2023**, *322*, 122127.
61. Tan, Z.; Zhang, J.; Yang, Y.; et al. Continuous Production of Formic Acid Solution from Electrocatalytic CO_2 Reduction Using Mesoporous Bi_2O_3 Nanosheets as Catalyst. *CCS Chem.* **2024**, *6*, 100–109.
62. Lin, L.; He, X.; Zhang, X.G.; et al. A Nanocomposite of Bismuth Clusters and $Bi_2O_2CO_3$ Sheets for Highly Efficient Electrocatalytic Reduction of CO_2 to Formate. *Angew. Chem. Int. Ed.* **2023**, *62*, e202214959.
63. Li, L.; Liu, Z.; Yu, X.; et al. Achieving High Single-Pass Carbon Conversion Efficiencies in Durable CO_2 Electroreduction in Strong Acids via Electrode Structure Engineering. *Angew. Chem. Int. Ed.* **2023**, *62*, e202300226.
64. Liu, G.; Zhong, Y.; Liu, Z.; et al. Solar-Driven Sugar Production Directly from CO_2 via a Customizable Electrocatalytic-Biocatalytic Flow System. *Nat. Commun.* **2024**, *15*, 2636.
65. Zhang, G.; Ji, N.; Lyu, S.; et al. Artificial Synthesis of Polyesters at Ambient Condition via Consecutive CO_2 Electrolysis and Fermentation. *Nano Res.* **2024**, *17*, 6016–6025.
66. Li, X.; Wang, J.H.; Yuan, C.Y.; et al. A Unique Amorphous Porous $BiSbO_x$ Nanotube with Abundant Unsaturated Sb-Stabilized BiO_{8-x} Sites for Efficient CO_2 Electroreduction in a Wide Potential Window. *Adv. Funct. Mater.* **2024**, *34*, 2402220.
67. Zhang, M.; Cao, A.; Xiang, Y.; et al. Strongly Coupled Ag/Sn–SnO_2 Nanosheets toward CO_2 Electroreduction to Pure HCOOH Solutions at Ampere-Level Current. *Nano-Micro Lett.* **2023**, *16*, 50.
68. Jia, B.; Chen, Z.; Li, C.; et al. Indium Cyanamide for Industrial-Grade CO_2 Electroreduction to Formic Acid. *J. Am. Chem. Soc.* **2023**, *145*, 14101–14111.